Pol. J. Environ. Stud. Vol. XX, No. X (XXXX), 1-13
DOI: *10.15244/pjoes/205506* ONLINE PUBLICATION DATE: 2025-07-28

Original Research

Study of the Reactive Red Dye (RR 120) Adsorption of Activated Carbon Prepared from Durian (*Durio zibethinus* Murr.) Peel

Tra Huong Do[1]*, Xuan Linh Ha[2], Van Kiet Doan[3], Quoc Khanh Le[3], Truong Xuan Vuong[4], Thi Cam Quyen Ngo[5]**

[1]Chemistry Faculty, Thai Nguyen University of Education, Thai Nguyen 250000, Vietnam
[2]International School, Thai Nguyen University, Thai Nguyen 250000, Vietnam
[3]Faculty of Natural Sciences, Tay Bac University, 250000, Vietnam
[4]Faculty of Chemistry, University of Science, Thai Nguyen University, Thai Nguyen 250000, Vietnam
[5]Institute of Applied Technology and Sustainable Development, Nguyen Tat Thanh University, Ho Chi Minh City, Vietnam

Received: 19 September 2024
Accepted: 24 May 2025

Abstract

The synthesis of activated carbon from durian peel activated with Na_2CO_3 (ACDSB) was achieved. Several factors affecting the adsorption capacity of Reactive Red dye (RR 120) on ACDSB-activated carbon by the static adsorption method were investigated. Results showed that the time to reach adsorption equilibrium was 30 minutes, the best adsorbent pH for RR 120 was 3, and the optimum mass of material was 2.5 g/L. The adsorption behavior of RR 120 on ACDSB adheres to the Langmuir, Freundlich, Tempkin, and Elovich isotherms of adsorption. The adsorption process of RR 120 on ACDSB-activated carbon follows the second-order kinetics equation, spontaneous, endothermic, physical, and chemical adsorption.

Keywords: activated carbon, RR 120, adsorption, aquatic environment, durian shell

Introduction

The presence of dyestuffs in industrial effluents stemming from sectors encompassing textiles, leather, paper, and plastics is a subject of paramount concern, owing to their deleterious repercussions on environmental integrity and human ecological systems. Due to the presence of toxic particulate matter, the effluent has elevated alkalinity, chromaticity, and organic substance content, directly leading to the extensive deployment of various chemical agents throughout the production process. Furthermore, certain dye compounds possess toxicological properties, culminating in carcinogenicity when they infiltrate consumable food and potable water sources, which pose substantial risks to human health upon exposure. The Reactive Red dye, RR 120, can be degraded to aromatic amines, which are carcinogenic under anaerobic conditions. Hence, dye removal from aquatic ecosystems is crucial in fostering a secure

*e-mail: huongdt.chem@tnue.edu.vn
**e-mail: ntcquyen@ntt.edu.vn

and pristine environment. Numerous methods have been utilized to eliminate azo dyes from industrial wastewater. These methods encompass a range of techniques, such as coagulation-flocculation [1], chemical and electrochemical oxidation [2], ozonation [3], ion exchange [4], and anaerobic-aerobic systems [5]. Nonetheless, these approaches are beset by practical challenges, including complexities in application, substantial capital investment prerequisites, and the necessity for costly chemical reagents [6].

Activated carbon (AC) is a frequently employed adsorbent in practical applications. This is primarily attributable to its finely tuned pore dimensions, the reactivity of surface functional moieties, and its expansive surface area, which affords an augmented number of adsorption binding sites [7-11].

The precursor material utilized for the synthesis is activated carbon lignocellulose. This material is a complex carbohydrate polymer comprising a diverse array of functional groups, with cellulose, lignin, and hemicellulose as the principal constituents. Phenolic and amino groups are responsible for pollutant adsorption. One of the priority areas that has recently attracted the interest of many scientists, both domestically and internationally, is the treatment of textile dyeing wastewater using activated carbon made from industrial and agricultural waste materials such as spent coffee [7, 12-16], neem leaves [17], tea waste [18-21], rice husks [18], mangosteen peels [21-25], fruit peel [26], bunch leaves moringa [27], and durian shell [9, 28-31].

Its main advantages include a rich source of materials, easy preparation, low cost, and environmental friendliness.

Durian trees are often grown in Southeast Asia, India, Sri Lanka, and Brunei. Durian peel is the residue from the durian fruit. The peel constitutes 70-85% of its total weight. Thus, it serves as a raw material for both manufacturing and investigating the adsorption of metal ions, dyes, and antibiotics in the aquatic environment. Current research on the adsorption of AC made from durian peel is very limited [9, 28, 29, 31, 32]. The works to make AC from durian peel are usually activated by H_3PO_4, H_2SO_4, and K_2CO_3 [32, 33]. Research on making AC from durian peel activated by Na_2CO_3 alone and the adsorption of dye RR 120 in an aqueous medium has not yet been studied.

The present study synthesized AC from durian shells through activation with Na_2CO_3 to adsorb RR 120. Activated carbon (AC) has been extensively studied, encompassing analysis of its morphological characteristics, surface functionalities, chemical composition, structural properties, and specific surface area. Several primary variables influencing the adsorption efficiency of RR 120 on manufactured activated carbon have been studied. Research several models of adsorption isotherms, kinetics, thermodynamics, and activation energy to gain insight into synthetic activated carbon's RR 120 adsorption process.

Materials and Methods

Chemicals

All chemicals employed in this study, including Na_2CO_3, RR 120, NaOH, and HCl, were Merck and of analytical grade with purity exceeding 99%.

RR 120 was with 99 % purity.

Making Activated Carbon from Durian Shell

Durian shells, upon procurement, underwent a rigorous cleansing procedure involving successive rinsing with tap water and distilled water to effectively eliminate any particulate matter. Subsequently, these cleaned durian shells were subjected to thermal treatment of 600ºC for 3 h, hereby referred to as DS for brevity. Then DS continued with chemical activation by Na_2CO_3 with mass ratio DS : Na_2CO_3 equal to 1:1, 2:1, and 3:2. It was then calcined at 600ºC for 3 h. After chemical activation, the resulting materials underwent a neutralization process using a hydrochloric acid (HCl) solution until the filtrate attained a state of neutrality. Subsequently, they were subjected to a drying procedure at a temperature of 110ºC for 24 h. The resulting product is designated as ACDSB. Finally, ACDSB was crushed and stored in glass vials for subsequent experiments.

Selection of Material Ratio DS : Na_2CO_3

Take 50 mL of RR 120 solution with a concentration of 47.85 mg/L (the concentration has been determined) and place it in a 100 mL conical flask containing 0.05 g of ACDSB material for the DS mass ratios : Na_2CO_3 equals 1:1, 2:1, 3:2, pH = 3. Shake in a shaker at 300 rpm at room temperature (25±10ºC) for 90 min. Then, centrifuge and determine the concentration of the active red 120 solution after adsorption. The results are shown in Table 1.

From Table 1, the adsorption efficiency of RR 120 clearly changes between the ratios of materials DS : Na_2CO_3. At a mass ratio of DS:Na_2CO_3 by 2:1, the adsorption efficiency of Active Red Food 120 reached the highest value of 90.18%. Therefore, the material DS : Na_2CO_3 with the ratio 2:1 (in terms of volume) was chosen to study and investigate the surface characteristics, structure, composition, specific surface area of the material, and adsorption capacity of RR 120 in aqueous medium.

Analysis of Physicochemical Properties of Activated Carbons DS and ACDSB

The fundamental characteristics of DS and ACDSB were investigated using a range of advanced equipment. SEM (transmission electron microscope) measurements were performed using the equipment JEM-2001F (Jeol, Tokyo, Japan). The EDX method, which determines sample composition, was performed

Table 1. Effects of mass ratios on the absorption efficiency RR 120.

No.	Mass ratios DS : Na_2CO_3	Adsorption Efficiency H (%)
1	1:1	80.79
2	2.1	90.18
3	3.2	83.68

on an MS-7001F device (Jeol, Tokyo, Japan). The FT-IR infrared spectrum was measured on a Shimadzu device made in Japan. The sample surface area was measured on a Tristar 3000 machine (Micromesitics). Crystallographic structures in the activated carbon sample were determined through X-ray diffraction (XRD) analysis utilizing a computer-controlled X-ray diffractometer (D2 Phraser; Brucker) fitted with a stepping motor and a graphite crystal monochromator.

The quantification of RR 120 concentrations both prior to and after adsorption was conducted utilizing a dual-beam UV-Vis 1700 (Shimadzu, Japan).

Experiment-Evaluated Factors Affecting the Adsorption Process

Solution pH, duration of exposure, mass of ACDSB, initial concentration of RR 120, and ambient temperature were systematically examined to assess the efficacy of RR 120 removal. The experimental procedure was replicated 3 times.

Study on the influence of pH: Add to each flask 0.05 g of ACDSB and 20 mL of RR 120 solution with the average initial concentration ranging from 60 mg/L to 70 mg/L (concentration has been determined exactly), whose pH varies from 3 to 10, stabilized by HNO_3 and NaOH solutions. Shake in a shaker for 90 min at 300 rpmat a temperature of 303 K. Then the solutions were centrifuged with a centrifuge at a speed of 4000 rpm for 30 min, using a micropipette to aspirate the solution after centrifugation and determine the concentration of RR 120 after adsorption.

The effect of time: Weigh 0.05 g of ACDSB into a 100 mL conical flask, then add the solution with an average concentration of 50-110 mg/L (concentration has been determined) to a 20 mL conical flask. The above solutions are kept stable at pH = 3. Shake for 5, 15, 30, 45, 60, and 90 min at 300 rpm at a temperature of 303 K.

Study on the influence of material weight: Weigh ACDSB into a 100 mL conical flask with a mass varying from 0.01 to 0.125g ACDSB, then add 20 mL of RR 120 solution with concentration in the flask. 54.26 mg/L (concentration has been determined). The above solutions are kept stable at pH = 3. Shake for 30 min at 300 rpm at 303 K.

The effect of temperature: 0.05 g of ACDSB was mixed with 20 mL of RR 120 solution with an average initial concentration of 104.45 mg/L in 100 mL Erlenmeyer flasks. Use KOH and HNO_3 to adjust the solution's pH to pH 3. Heat the solutions on a heated magnetic stirrer for 5-45 min at a shaking speed of 300 rpm at the respective temperature values of 303 K, 313 K, and 323 K.

The effect of concentration: Add 0.05 g of ACDSB and 20 mL of RR 120 solution to each conical flask with an average initial concentration of 50-500 mg/L (concentration has been determined). The above solutions were kept stable at pH 3 with HNO_3 solution. Shake for 30 min at 300 rpm at 303 K.

The adsorption effectiveness of RR 120 on activated carbon (ACDSB) was computed using the ensuing formula (1):

$$H = \frac{(C_o - Ce)}{C_o} \times 100 \quad (1)$$

Where H is adsorption efficiency, C_0 is the initial solution concentration (mg/L), and C_e is the solution concentration when reaching adsorption equilibrium (mg/L).

ACDSB material then determined some physical parameters, the isoelectric point, and studied isotherm adsorption models, including the Langmuir, Freundlich, Dubinin-Radushkevich (D-R), Tempkin, Elovich, adsorption kinetics, activation energy, and thermodynamics, according to Quoc Toan Tran et al. (2022) [30].

Results and Discussion

Selection of Material Ratio DS : Na_2CO_3

The results are shown in Table 2.

From Table 2, the adsorption efficiency of RR 120 clearly changes between the ratios of materials DS : Na_2CO_3. At a mass ratio of DS : Na_2CO_3 by 2:1, the adsorption efficiency of RR 120 reached the highest value of 90.18 %. Therefore, the material DS : Na_2CO_3 with the ratio 2:1 (in terms of volume) was chosen to study and investigate the surface characteristics, structure, composition, specific surface area of the material, and adsorption capacity of RR 120 in aqueous medium.

Table 2. Effects of mass ratios of DS : Na_2CO_3 on the absorption efficiency RR120.

No.	Mass ratios DS : Na_2CO_3	Adsorption Efficiency H (%)
1	1:1	80.79
2	2.1	90.18
3	3.2	83.68

Study of the Physical Attributes and Surface Properties of Activated Carbons DS and ACDSB

SEM images depicting DS and ACDSB materials are illustrated in Fig. 1 and Fig. 2.

Fig. 2 shows that after treatment with Na_2CO_3, the surface morphology of the durian peel underwent significant alteration compared to its untreated state. Prior to activation, the DS material displayed a surface characterized by varying degrees of smoothness, roughness, and reduced porosity (Fig. 1). After being activated with Na_2CO_3, the ACDSB material has formed tubular capillaries, creating additional voids and enhancing surface porosity, leading to potential applications as better adsorbents (Fig. 2). ACDSB-activated carbon incorporating Na_2CO_3 exhibited superior porosity compared to ACDSB-activated carbon derived from durian peels and activated using H_2SO_4 [20], which the authors have previously researched and published.

The results of the EDS energy scattering spectroscopy analysis of ACDSB materials are shown in Table 3. From the results, the carbon content of ACDSB was notably elevated in terms of mass (87.86%) and low oxygen content by mass (8.41%). Compared with and relative to activated carbon synthesized using H_2SO_4-activated durian shell (ACDS) (Table 3), ACDSB material activated with Na_2CO_3 had a higher carbon content than ACDS material [30].

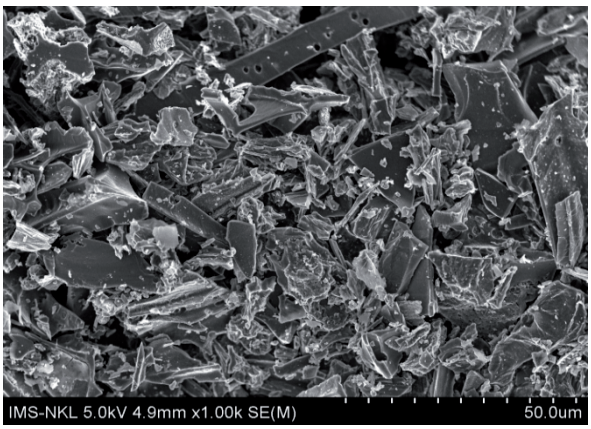

Fig. 1. SEM image of DS material.

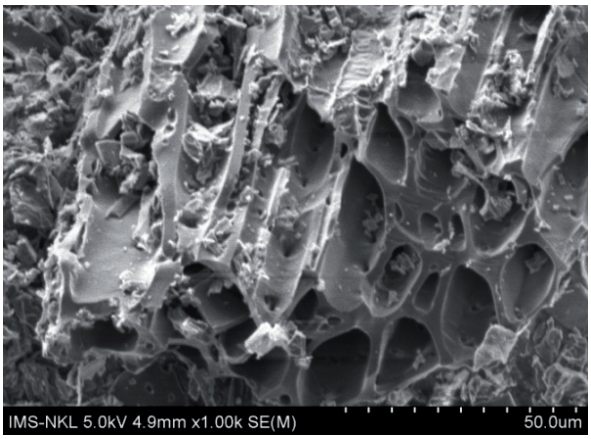

Fig. 2. SEM image of ACDSB materials.

FT-IR spectroscopy, as depicted in Fig. 3, was employed to investigate the surface functional groups of ACDSB. The findings demonstrated a significant peak at 3732.26 cm^{-1}, which signifies the -OH group. The spectral pattern at about 2980.02 and 2897.08 cm^{-1} was assigned to the C–H stretching vibration of the methylene group ($–CH_2$), the spectral pattern at 2133.27 cm^{-1} was assigned to the C–C vibration of the alkyne group (–C=C–), and the range from 1791.87 to 1994. 40 cm^{-1} was assigned the C=O oscillations of saturated fatty esters and carboxylic acids, with strong peaks at 1680.00 and 1556.55 cm^{-1}, possibly due to prolonged oscillations of C=C and C=O in organic matter. The absorption peak observed between 1300-900 cm^{-1} was assigned to the C–N and C–O stretching oscillation. This is consistent with the EDX analysis results, which show that the main components of ACDSB and ACDS materials are C and O [20].

The results of XRD spectrometry of ACDSB coal are shown in Fig. 4. Fig. 4 results show that the C (002) diffraction peak is wide (2θ = 22-30º), and the C (101) diffraction peak is weak and wide (2θ = 40-50º) and can be attributed to the amorphous carbon structures. From this structural feature, activated carbon has an amorphous carbon structure [19].

The ACDSB material has a specific surface area of 497.00 m^2/g, which shows that its surface area is large. Compared with ACDS material, ACDSB material has a larger specific surface area than ACDS (348.00 m^2/g) [30].

The analysis results show that ACDSB has higher porosity, carbon content, and specific surface area than ACDS.

Determining the Isoelectric Point of ACDSB

Fig. 5 presents the outcomes of the isoelectric point determination for ACDSB. The analysis results indicate that ACDSB exhibits greater porosity, carbon content, and specific surface area than ACDS.

The results of Fig. 6 determined the isoelectric point (pH_{pzc}) of ACDSB pH_{pzc} = 6.9. These findings indicate that ACDSB exhibited a positive surface charge at pH levels below pH_{pzc} and shifted to a negative charge as pH surpassed the pH_{pzc} threshold.

Results of Physical Parameters and the Iodine Index of ACDSB

Table 4 displays the physical characteristics of ACDSB and ACDS.

ACDSB-activated carbon exhibits notably diminished moisture content and a correspondingly reduced density. In terms of its mechanical attributes,

Table 3. Analysis Results of ACDSB and ACDS Materials Using Energy Dispersive X-ray Spectroscopy.

ACDSB			ACDS [30]		
Element	% Mass	% Atom	Element	% Mass	% Atom
C	87.86	91.91	C	82.08	87.06
O	8.41	6.61	O	15.09	12.02
Mg	1.14	0.59	Cl	0.17	0.06
P	0.85	0.34	K	2.66	0.87
K	0.50	0.16	Total	100.00	100.00
Total	100.00	100.00			

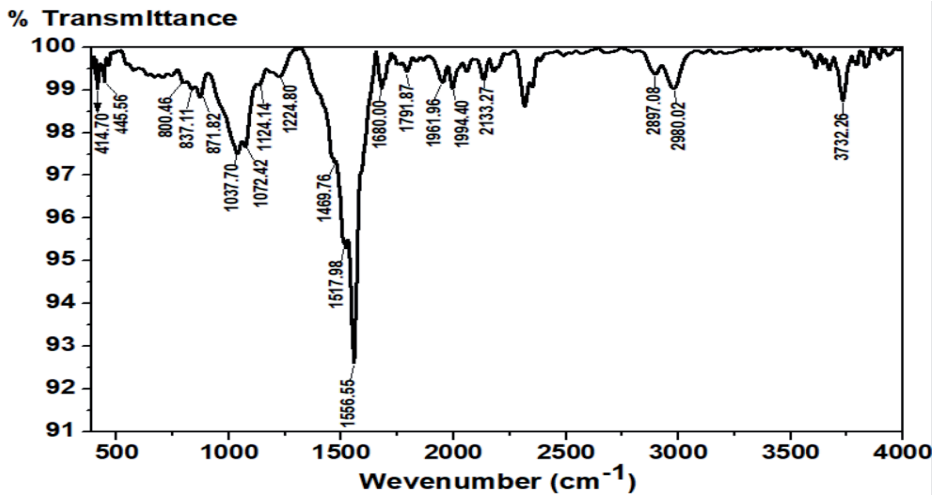

Fig. 3. FT-IR infrared spectrum of ACDSB.

this feature is an advantageous characteristic of ACDSB-derived activated carbon. The elevated moisture content can significantly compromise the thermal engineering properties of activated carbon, and its structural integrity and overall durability are diminished. This result also shows that the physical parameters of ACDSB are better than ACDS. The iodine index of ACDSB material is 709 mg/g and higher than that of ACDS material (634 mg/g) [30].

The results of the investigation of factors affecting the adsorption capacity of RR 120 on ACDSB

Effect of pH

Fig. 6 shows that both adsorption efficiency and capacity increase with lower pH. This can be explained

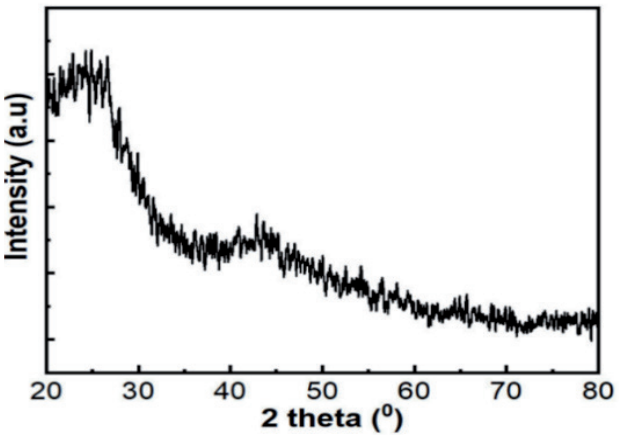

Fig. 4. X-ray diffraction patterns of ACDSB material.

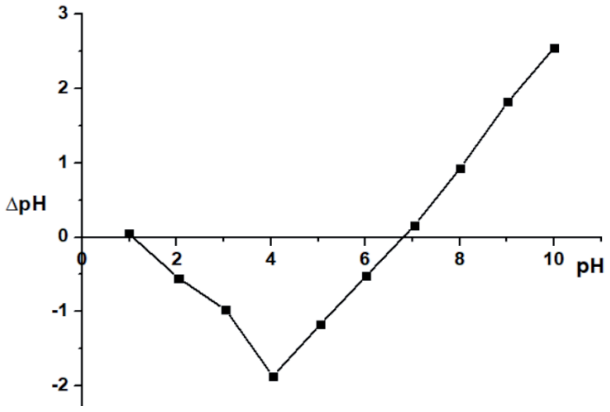

Fig. 5. The isoelectric point of ACDSB.

Table 4. Analysis of Activated Carbons ACDSB and ACDS Based on Physical Parameters.

Parameters	ACDSB	ACDS [30]
Ash content (%)	56.16±0.5	55.63±1
Moisture content (%)	2.1±0.05	4.74±0.03
Density (g/cm^3)	0.65±0.05	0.83±0.05

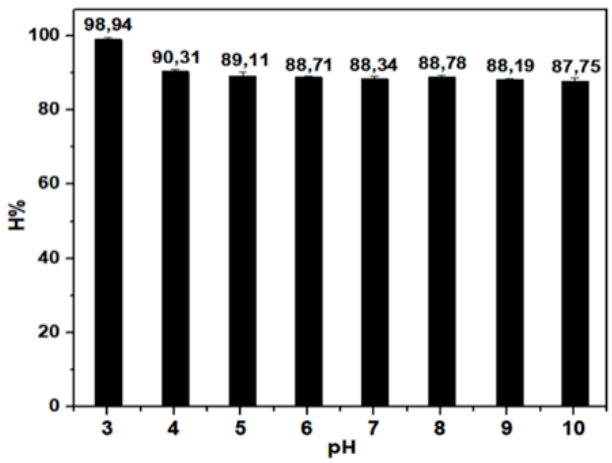

Fig. 6. The effect of pH on the adsorption efficiency of RR 120.

by the fact that, at low pH values, electrostatic attraction between the positive charge on the surface of ACDSB and the sulfate groups RR-120 (D-SO_3Na) has been dissociated into anions (D-SO_3-). When the pH value is high, a repulsive force appears between the surface of the negatively charged ACDSB material and the anion (D-SO_3). Therefore, the best adsorption pH for ACDSB's RR 120 solution was selected as pH 3 and used for further experiments.

Effect of Adsorption Time

Fig. 7 illustrates a notable rise in adsorption efficiency from 5 to 30 min, followed by a nearly linear progression and subsequent stabilization between 30 and 90 min. Therefore, the time to reach adsorption equilibrium is 30 min. These results were used for subsequent experiments.

Effect of ACDSB Mass

As illustrated in Fig. 8, there is a discernible augmentation in RR 120 adsorption efficiency as the mass of ACDSB escalates. Importantly, this enhancement exhibits a linear correlation within the scope of investigated adsorbed ACDSB material weights. However, in the weight range of ACDSB, which increased from 0.05 to 0.125 g, the adsorption efficiency did not increase much (from 96.11 to 98.16%). Therefore, we chose an ACDSB mass of 0.05 g for further studies.

Effect of Temperature

Fig. 9 shows that increasing temperature decreases both adsorption efficiency and adsorption capacity. Given that adsorption constitutes an endothermic process, elevating the temperature results in a thermodynamic shift of the adsorption equilibrium towards the right, thereby diminishing the adsorbate concentration within the solution.

Model of Adsorption Isotherm

Langmuir Isotherm Adsorption Model

Fig. 10a) shows that the maximum adsorption capacity and constant were determined [30] as q_{max} = 46.51 mg/g and b = 0.056 (L/g), respectively. The calculated R_L parameter values shown in Fig. 10b)

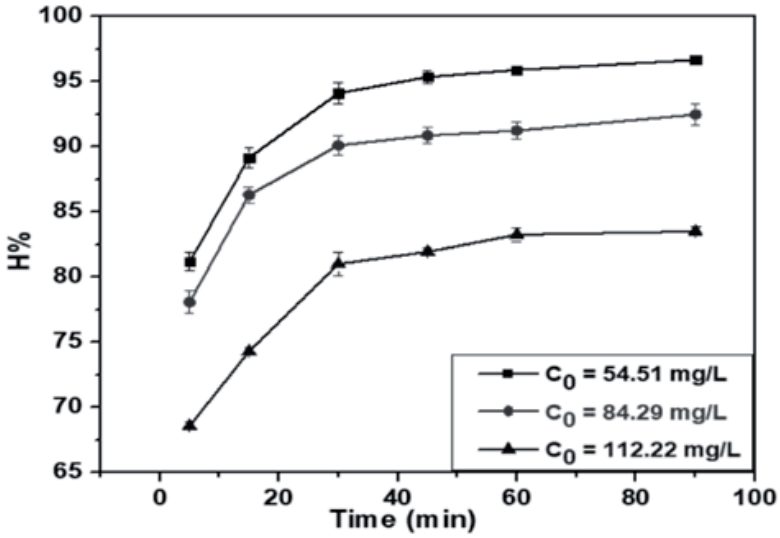

Fig. 7. The effect of time on the adsorption efficiency of RR 120.

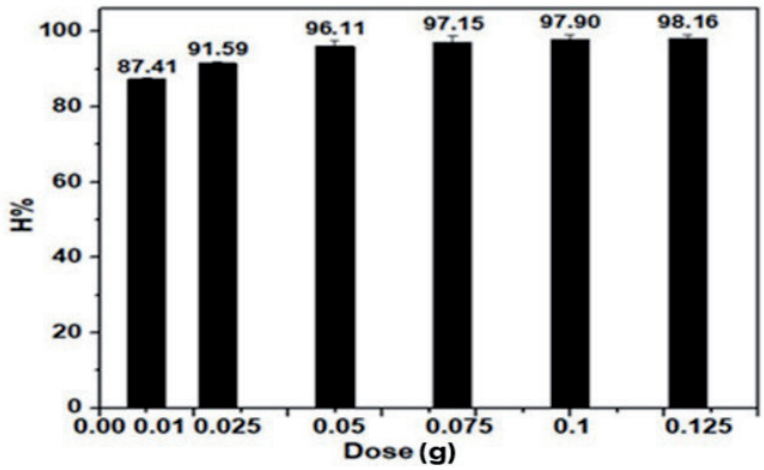

Fig. 8. The effect of ACDSB mass on the adsorption efficiency of RR 120.

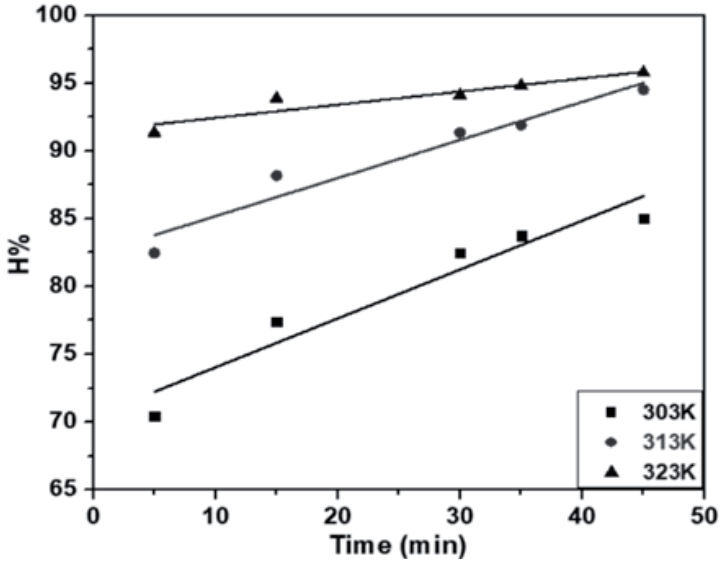

Fig. 9. The effect of ACDSB time on the adsorption efficiency of RR 120 at different temperatures.

indicate that the R_L values ranging from 0.24 to 0.03 were all less than 1. Therefore, it is evident that the Langmuir isotherm model appropriately characterizes the adsorption process of RR 120 on ACDSB materials.

Examination of the adsorption capabilities of RR 120 across varied materials (Table 5) reveals that ACDSB-activated carbon exhibited a maximum adsorption capacity (q_{max}) for RR 120 that closely resembled that of synthetic materials of comparable nanometer scales [29, 33], higher than polyamide nylon 6 microplastic material.

Freundlich Isotherm Model of Adsorption

Fig. 11 shows the Freundlich isotherm model describing the adsorption process of RR 120 on adsorbed ACDSB. The Freundlich adsorption constant was calculated as K_F = 14.12 (L/g) and n = 4.81. The correlation coefficient R^2 = 0.9733. Large K_F and n values indicate activated carbon's good adsorption capacity and show an adsorption bond between adsorbent and adsorbent.

Dubinin-Radushkevich Isotherm Adsorption Model

As shown in Fig. 12, the correlation coefficient (R^2) derived from the D-R isotherm model is notably small (R^2 = 0.6953). Consequently, it can be inferred that the D-R isotherm model does not adequately suit the adsorption dynamics of RR 120 onto the activated carbon derived from durian shell (ACDSB).

Tempkin Isotherm Adsorption Model

According to the findings illustrated in Fig. 13, the coefficient of determination R^2 was determined to be 0.985. Therefore, the adsorption process of RR 120 on ACDSB was consistent with the Tempkin model.

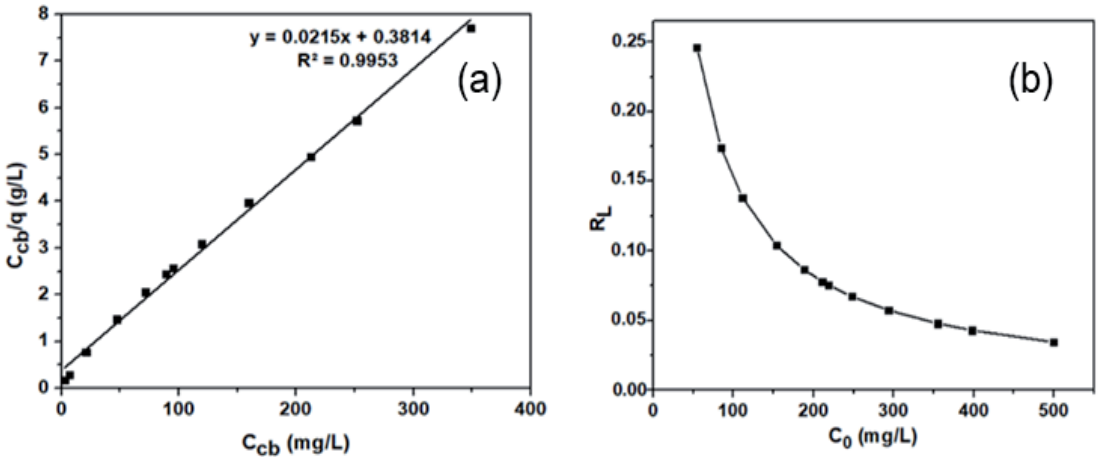

Fig. 10. a) The effect of C_{cb}/q on C_{cb}; b) the parameter value R_L with C_o.

Table 5. Maximum absorption capacity RR 120 of various materials.

No.	Adsorption materials	Maximum adsorption capacity (mg/g)	Reference
1	Activated carbon made from herbal waste	47.88	[32]
2	Fe_3O_4 magnetic nanoparticles	49.26	[33]
3	Mg-hydrotalcites	45.94	[34]
4	Polyamide Nylon 6 Microplastics	3.96	[35]
5	Durian shell	46.51	This project

Elovich Isotherm Adsorption Model

The application of the Elovich adsorption isotherm model pertains to the process of multilayer adsorption. Fig. 14 showed that qmax was 7.67 mg/g and K_e was 6.39.

Overall, the Langmuir, Freundlich, Dubinin-Radushkevich, Tempkin, and Elovich models demonstrated R^2 values of 0.9911, 0.9733, 0.6953, 0.9895, and 0.9845, respectively.

The adsorption process of RR 120 on ACDSB-activated carbon adheres to the Langmuir, Freundlich, Tempkin, and Elovich adsorption isotherm models. Adsorption occurs via multilayer mechanisms amid the activated carbon's non-uniform surface, where significant interactions between adsorbent and adsorbate are evident [21, 23, 27, 31].

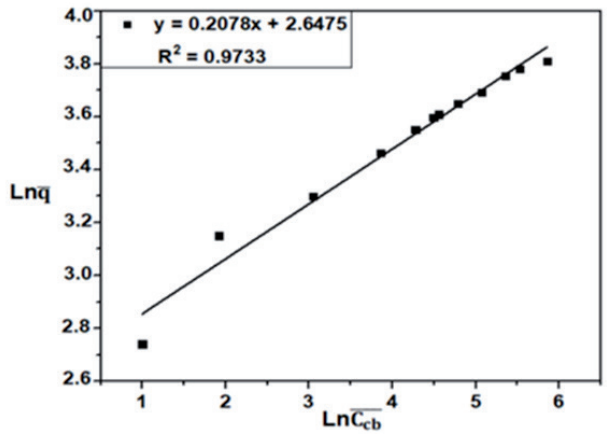

Fig. 11. The effect of Lnq on LnC_{cb} for RR 120 adsorption.

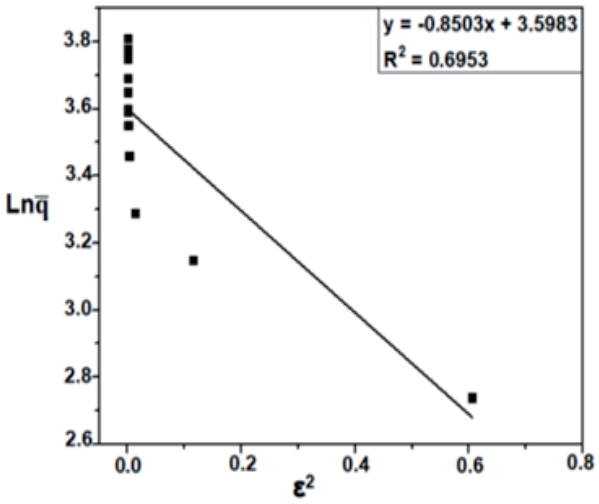

Fig. 12. The effect of Lnq^- on ε^2

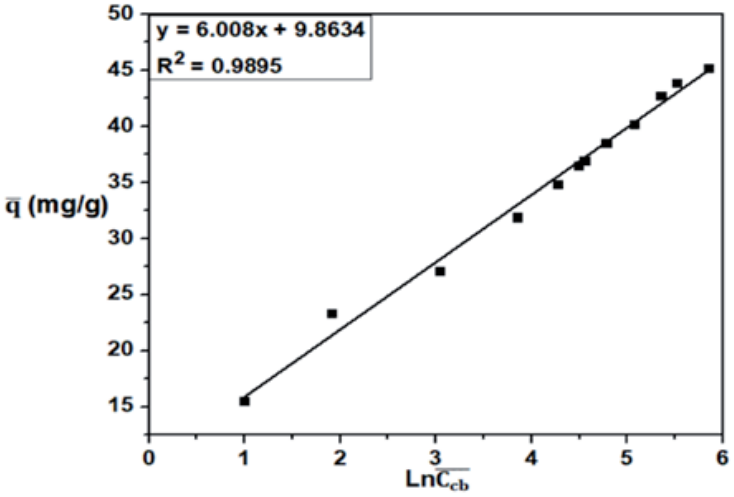

Fig. 13. The effect of $\bar{q}$ on $Ln\bar{C}cb$ according to the Tempkin model.

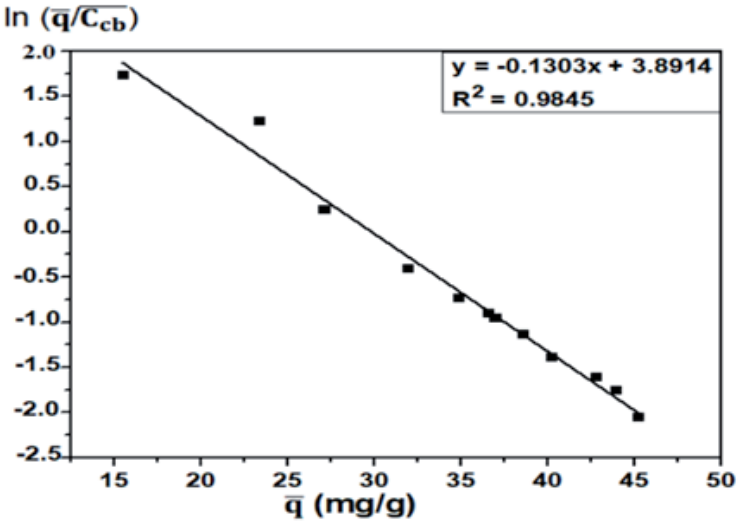

Fig. 14. The impact of ln (q/Ccb) on $\bar{q}$.

Adsorption Kinetic Models

Tables 6 and 7 display the findings from the kinetic analysis of the RR 120 adsorption process on ACDSB-activated carbon. The values of the kinetic parameters from the first-order kinetic equation in Table 5 and Fig. 15a) indicate that the coefficient of determination (R^2) falls within the range of 0.7453 to 0.8556. Furthermore, a noticeable disparity exists between the experimentally determined adsorption capacity and the calculated capacity derived from the kinetic equations. Hence, the first-order kinetic equation is not suitable for describing the adsorption process of RR 120 onto ACDSB.

The values in Table 6 and the graph in Fig. 15b) show that the coefficient of determination (R^2) is consistently high, exceeding 0.99. Additionally, the experimentally determined adsorption capacities closely align with

Table 6. Parameter values of the first-order adsorption kinetic aquation.

Red product concentration RR 120 (mg/L)	q_e, experiment (mg/g)	q_e, calculate (mg/g)	Constant k_1 (min^{-1})	R^2
54.50	15.99	9.99	0.281	0.8556
86.33	21.58	14.07	0.197	0.8845
110.25	25.34	16.28	0.138	0.7453

Table 7. Parameter values of the second-order adsorption kinetic aquation.

Red product concentration RR 120 (mg/L)	q_e, experiment (mg/g)	q_e, calculate (mg/g)	Constant k_2 (min^{-1} L mg^{-1})	R^2
54.50	16.69	17.32	0.0511	1
86.33	23.98	24.48	0.0287	1
110.25	27.54	28.25	0.0150	0.99903

the results obtained by applying kinetic equations. Thus, it can be deduced that the pseudo-second-order kinetic equation is well-suited for elucidating the adsorption mechanism of RR 120 on ACDSB.

The Weber and Morris intraparticle diffusion model reveals that the plot of q_t as a function of $t^{0.5}$ can be divided into two regions (Fig. 16a)). Region 1, the initial portion, is attributed to the diffusion of the adsorbate from the bulk solution to the external surface of the adsorbent (external surface adsorption). Region 2 describes the adsorption stage, where intraparticle diffusion plays a decisive role in the adsorption rate to the solid phase surface of the ACDSB. Moreover, the linear plots observed in Region 2 do not cross the origin, suggesting that factors beyond intraparticle diffusion contribute to determining the adsorption rate [17, 20].

The liquid film diffusion model illustrates that Ln(1-F), as a function of time, exhibits a linear graph

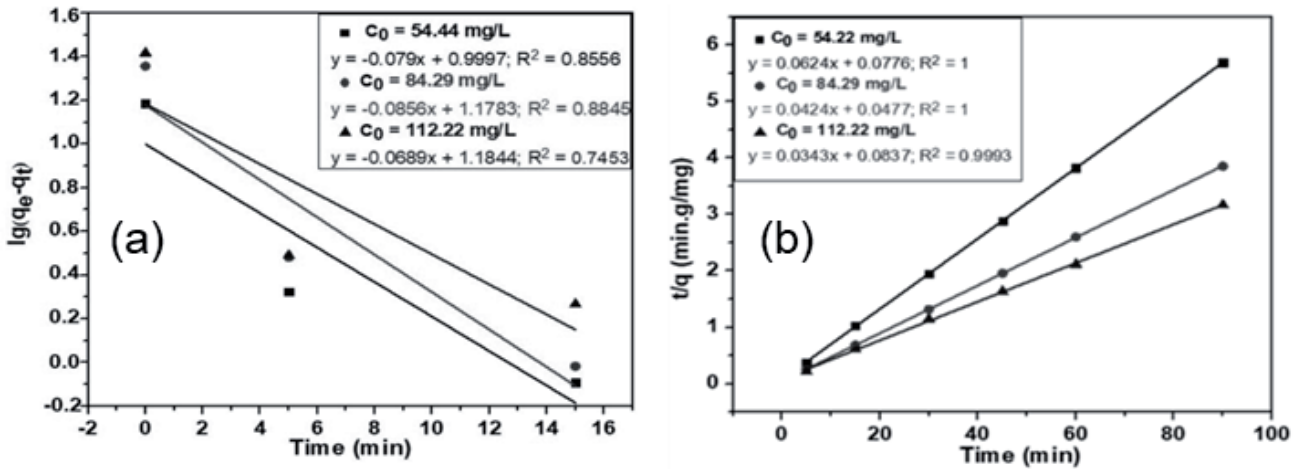

Fig. 15. a) The first-order and b) the second-order kinetic equation for RR 120.

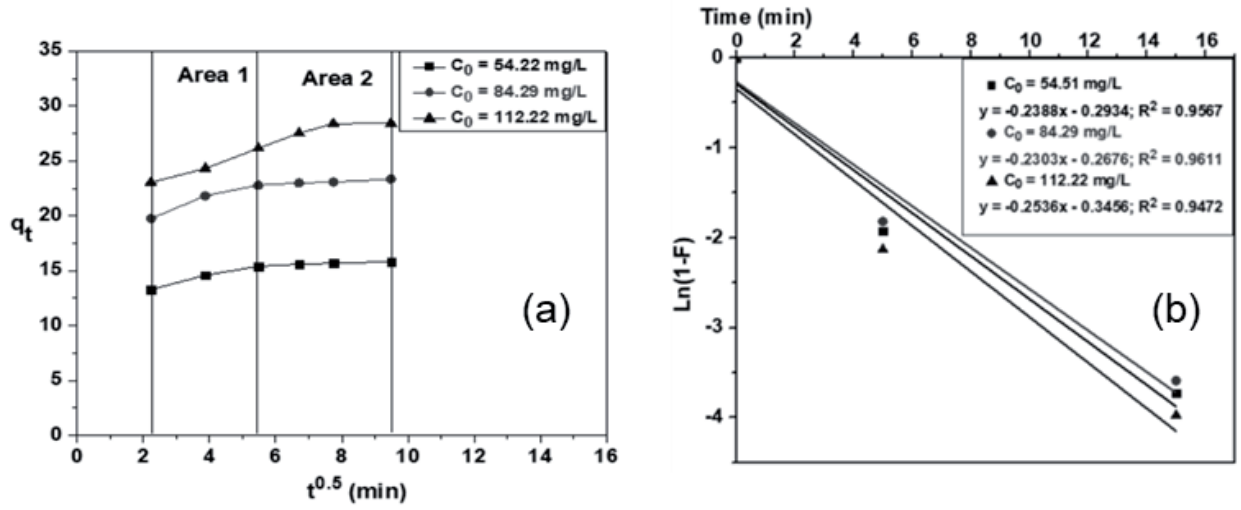

Fig. 16. a) q_t depends on time $t^{0.5}$ and b) Ln(1-F) on time.

Table 8. Activation energy parameter values.

Concentration of RR 120 (mg/L)	Second-order kinetics equation	Constant k_2 (g/mg min)	h	E (kJ/moL)
54.50	$t/q_t = 0.0624x + 0.0786$	0.0511	11.88	14.54
86.33	$t/q_t = 0.0424x + 0.0577$	0.0287	20.96	15.72
110.25	$t/q_t = 0.0343x + 0.0937$	0.0150	12.94	16.72

(Fig. 16b)). Hence, film diffusion emerges as a pivotal determinant of the adsorption rate.

The membrane diffusion model for the liquid indicates that the plot of Ln(1-F) over time exhibited a linear relationship, so membrane diffusion determines the rate in the adsorption process (Fig. 16b)). Consequently, the thick diffusion film enveloping the ACDSB impeded RR 120 migration from the liquid phase to the solid phase surface of the ACDSB. Hence, membrane diffusion predominated in the adsorption of ACDSB on ACDS-activated carbon [17, 18].

Activation Energy

Table 8 displays the findings concerning the RR 120 adsorption activation energy of ACDSB-activated carbon. Analysis revealed that E<25 kJ/mol, suggesting that external diffusion governed the RR 120 adsorption process on ACDS.

RR 120 Adsorption Thermodynamics of ACDSB Materials

The findings from the thermodynamic analysis of the RR 120 adsorption process using ACDSB-activated carbon are detailed in Table 9.

From Table 9, it can be seen that: The free energy change (ΔG^0) obtained has a negative value from -1.110 to -4.224 kJ/mol, and the entropy change (ΔS^0) has a positive value of 0.1607 kJ/mol, which proves the adsorption process ACDSB's RR 120 is spontaneous. The measured enthalpy change (ΔH^0) was 47.68 kJ/mol positive, signifying the adsorption process as being endothermic.

Zhang et al. [25] have shown that: In the adsorption process, if $\Delta H^o < 25$ kJ/mol, van der Waals forces were the main interactions leading to physical adsorption. For ΔH^o valued in the range of 40 to 200 kJ/mol, chemical bonding predominantly drives chemisorption in the material. Therefore, the results of thermodynamic calculations (Table 9) show that the adsorption process of RR 120 was chemisorption.

Table 9. Thermodynamic parameters for the RR120 adsorption process.

T (K)	ΔG^0 (kJ/mol)	ΔH^0 (kJ/mol)	ΔS^0 (kJ/mol K)
303	-1.010	47.68	0.1607
313	-3,003		
323	-4.224		

Conversely, the findings from the investigation into the adsorption dynamics of RR 120 onto ACDSB materials conform to the second-order apparent kinetics equation and align with the Tempkin and Elovich adsorption isotherm models. This observation suggests that the interaction between RR 120 and ACDSB is governed by chemisorptive forces, indicating a propensity for chemical adsorption processes. This trend notably parallels the outcomes of thermodynamic calculations and bears a resemblance to prior research on the adsorption of Methylene Blue (MB) onto ACDS-activated carbon treated with sulfuric acid (H_2SO_4) [18].

Conclusions

The current investigation involves the production of activated carbon derived from durian shells, activated using sodium carbonate (ACDSB). The fabricated ACDSB activated carbon has a porous surface, micro-capillary size, a specific surface area of 497.00 m^2/g, an ash level of 56.16 %, humidity of 2.1%, density of 0.65 g/cm^3, an iodine index of 709 mg/g, and an isoelectric point of 6.9. Various parameters influencing the adsorption efficiency of RR 120 onto ACDSB materials were examined using a static adsorption technique. The results indicated that pH 3 yielded the highest adsorption capacity for RR 120; reaching adsorption equilibrium took 30 min, and the mass/volume ratio was 2.5g/L. When increasing the temperature in the range of 303-323 K, the adsorption efficiency increased. The adsorption process of RR 120 on ACDSB material followed the Langmuir, Freundlich, Tempkin, and Elovich isotherm adsorption model. The maximum adsorption capacity for RR 120 on ACDSB was $q_{max} = 46.51$ mg/g. The adsorption process of RR 120 on ACDSB material follows the apparent second-order kinetics equation. The adsorption rate was primarily governed by intra-particle and membrane diffusion, as well as the spontaneous, endothermic, physical, and chemical interactions occurring during adsorption.

Conflict of Interest

The authors declare no conflict of interest.

References

1. OBIORA-OKAFO I., ONUKWULI O. Optimization of coagulation-flocculation process for colour removal from azo dye using natural polymers: Response surface methodological approach. Nigerian Journal of Technology. **36** (2), 482, **2017**.
2. ISARAIN-CHÁVEZ E., BARÓ M.D., ROSSINYOL E., MORALES-ORTIZ U., SORT J., BRILLAS E., PELLICER E. Comparative electrochemical oxidation of methyl orange azo dye using Ti/Ir-Pb, Ti/Ir-Sn, Ti/Ru-Pb, Ti/Pt-Pd and Ti/RuO2 anodes. Electrochimica Acta. **244**, 199, **2017**.
3. CASTRO F.D., BASSIN J.P., DEZOTTI M. Treatment of a simulated textile wastewater containing the Reactive Orange 16 azo dye by a combination of ozonation and moving-bed biofilm reactor: evaluating the performance, toxicity, and oxidation by-products. Environmental Science and Pollution Research. **24**, 6307, **2017**.
4. JOSEPH J., RADHAKRISHNAN R.C., JOHNSON J.K., JOY S.P., THOMAS J. Ion-exchange mediated removal of cationic dye-stuffs from water using ammonium phosphomolybdate. Materials Chemistry and Physics. **242**, 122488, **2020**.
5. BAHIA M., PASSOS F., ADARME O.F., AQUINO S.F., SILVA S.Q. Anaerobic-Aerobic Combined System for the Biological Treatment of Azo Dye Solution using Residual Yeast: Bahia et al. Water Environment Research. **90** (8), 729, **2018**.
6. GOPALAKRISHNAN Y., AL-GHEETHI A., ABDUL MALEK M., MARISA AZLAN M., AL-SAHARI M., RADIN MOHAMED R.M.S., ALKHADHER S., NOMAN E. Removal of basic brown 16 from aqueous solution using durian shell adsorbent, optimisation and techno-economic analysis. Sustainability. **12** (21), 8928, **2020**.
7. FIGUEROA CAMPOS G.A., PEREZ J.P.H., BLOCK I., SAGU S.T., SARAVIA CELIS P., TAUBERT A., RAWEL H.M. Preparation of activated carbons from spent coffee grounds and coffee parchment and assessment of their adsorbent efficiency. Processes. **9** (8), 1396, **2021**.
8. AMIR D., NASARUDDIN R.R., YOUSEFI M., MASTULI M.S., SULAIMAN S., ALAM M.Z., ENGLIMAN N.S. Investigating the synthesis parameters of durian skin-based activated carbon and the effects of silver nanocatalysts on its recyclability in methylene blue removal. Discover Nano. **19** (1), 32, **2024**.
9. DAMAYANTI A., WULANSARIE R., BAHLAWAN Z.A.S., SUHARTA ROYANA M., BASUKI M.W.N.M., NUGROHO B., ANDRI A.L. Effects of Phosphate and Thermal Treatments on the Characteristics of Activated Carbon Manufactured from Durian (Durio zibethinus) Peel. ChemEngineering. **7** (5), 75, **2023**.
10. CAMPBELL R., XIAO B., MANGWANDI C. Production of activated carbon from spent coffee grounds (SCG) for removal of hexavalent chromium from synthetic wastewater solutions. Journal of Environmental Management. **366**, 121682, **2024**.
11. MADHU R., SANKAR K.V., CHEN S.-M., SELVAN R.K. Eco-friendly synthesis of activated carbon from dead mango leaves for the ultrahigh sensitive detection of toxic heavy metal ions and energy storage applications. Rsc Advances. **4** (3), 1225, **2014**.
12. CUCCARESE M., BRUTTI S., DE BONIS A., TEGHIL R., DI CAPUA F., MANCINI I. M., MASI S., CANIANI D. Sustainable adsorbent material prepared by soft alkaline activation of spent coffee grounds: characterisation and adsorption mechanism of methylene blue from aqueous solutions. Sustainability. **15** (3), 2454, **2023**.
13. MILANKOVIĆ V., TASIĆ T., PEJČIĆ M., PAŠTI I., LAZAREVIĆ-PAŠTI T. Spent coffee grounds as an adsorbent for malathion and chlorpyrifos – Kinetics, thermodynamics, and eco-Neurotoxicity. Foods. **12** (12), 2397, **2023**.
14. CASTRO L.E.N.D., BATTOCCHIO D.A.J., RIBEIRO L.F., COLPINI L.M.S. Development of adsorbent materials using residue from coffee industry and application in food dye adsorption processes. Brazilian Archives of Biology and Technology. **66**, e23210125, **2022**.
15. SKORUPA A., WORWĄG M., KOWALCZYK M. Coffee Industry and ways of using by-products as bioadsorbents for removal of pollutants. Water. **15** (1), 112, **2022**.
16. AKINDOLIE M., CHOI H. Surface modification of spent coffee grounds using phosphoric acid for enhancement of methylene blue adsorption from aqueous solution. Water Science and Technology. **85** (4), 1218, **2022**.
17. MUSTAFA S.K., AL-AOH H.A., BANI-ATTA S.A., ALRAWASHDEH L.R., ALJOHANI M.M., ALSHARIF M.A., DARWISH A., AL-SHEHRI H., AHMAD M.A., AL-TWEHER J.N. Enhance the adsorption behavior of methylene blue from wastewater by using $ZnCl_2$ modified neem (Azadirachta indica) leaves powder. Desalination and Water Treatment. **209**, 367, **2021**.
18. HONGO T., MORIURA M., HATADA Y., ABIKO H. Simultaneous methylene blue adsorption and pH neutralization of contaminated water by rice husk ash. ACS Omega. **6** (33), 21604, **2021**.
19. KABIR M.M., MOUNA S.S.P., AKTER S., KHANDAKER S., DIDAR-UL-ALAM M., BAHADUR N.M., MOHINUZZAMAN M., ISLAM M.A., SHENASHEN M. Tea waste based natural adsorbent for toxic pollutant removal from waste samples. Journal of Molecular Liquids. **322**, 115012, **2021**.
20. DEBNATH B., HALDAR D., PURKAIT M.K. Environmental remediation by tea waste and its derivative products: a review on present status and technological advancements. Chemosphere. **300**, 134480, **2022**.
21. TRAN Q.T., DO T.H., HA X.L., NGUYEN H.P., NGUYEN A.T., NGO T.C.Q., CHAU H.D. Study of the ciprofloxacin adsorption of activated carbon prepared from mangosteen peel. Applied Sciences. **12** (17), 8770, **2022**.
22. KONGSUNE P., RATTANAPAN S., CHANAJAREE R. The removal of Pb^{2+} from aqueous solution using mangosteen peel activated carbon: Isotherm, kinetic, thermodynamic and binding energy calculation. Groundwater for Sustainable Development. **12**, 100524, **2021**.
23. HANAMI Z.A., LESTARI P. Characterization and application of mangosteen peel activated carbon for ammonia gas removal. Environment and Natural Resources Journal. **19** (4), 320, **2021**.
24. GIRALDO L., MORENO-PIRAJÁN J.C. CO_2 adsorption on activated carbon prepared from mangosteen peel: Study by adsorption calorimetry. Journal of Thermal Analysis and Calorimetry. **133**, 337, **2018**.
25. ZHANG Z., XU L., LIU Y., FENG R., ZOU T., ZHANG Y., KANG Y., ZHOU P. Efficient removal of methylene blue using the mesoporous activated carbon obtained from mangosteen peel wastes: Kinetic, equilibrium, and thermodynamic studies. Microporous and Mesoporous Materials. **315**, 110904, **2021**.

26. PRAIPIPAT P., NGAMSURACH P., BUNCHU K., LEKWAREE V., SRIRAT P., CHAIPHUMEE P., NOISRI J., AEAMSA-ARD T. Comparative performance of fruit peel materials for methylene blue dye adsorption. International Journal of Environmental Science and Technology. **22** (9), 1, **2024**.
27. DO T.H., DUNG N.Q., CHU M.N., VAN KIET D., NGAN T.T.K., VAN TAN L. Study on methylene blue adsorption of activated carbon made from Moringa oleifera leaf. Materials Today: Proceedings. **38**, 3405, **2021**.
28. SUDRAJAT H., SUSANTI A., PUTRI D.K.Y., HARTUTI S. Mechanistic insights into the adsorption of methylene blue by particulate durian peel waste in water. Water Science and Technology. **84** (7), 1774, **2021**.
29. YULIUSMAN Y., PUTRI S.A., SIPANGKAR S.P., FATKHURRAHMAN M., FAROUQ F.A. Utilization of durian shell waste in the preparation of activated carbon by using K_2CO_3 as chemical activator. AIP Conference Proceedings. **2255** (1), 060027, **2020**.
30. TRAN Q.T., ĐO T.H., HA X.L., DUONG T.T.A., CHU M.N., VU V.N., CHAU H.D., TRAN T.K.N., SONG P. Experimental design, equilibrium modeling and kinetic studies on the adsorption of methylene blue by adsorbent: activated carbon from durian shell waste. Materials. **15** (23), 8566, **2022**.
31. MUSTHAPA S.M.B.H., SHAMS S., PRASAD D.R. Removal of pollutants from wastewater using activated carbon from durian peel. IOP Conference Series Earth and Environmental Science. **1135** (1), 012001, **2023**.
32. BAZRAFSHAN E., AHMADABADI M., MAHVI A.H. Reactive Red-120 removal by activated carbon obtained from cumin herb wastes. Fresenius Environmental Bulletin. **22** (2a), 584, **2013**.
33. ABSALAN G., ASADI M., KAMRAN S., SHEIKHIAN L., GOLTZ D.M. Removal of reactive red-120 and 4-(2-pyridylazo) resorcinol from aqueous samples by Fe_3O_4 magnetic nanoparticles using ionic liquid as modifier. Journal of Hazardous Materials. **192** (2), 476, **2011**.
34. DÁVILA I.J., ROSSET M., LOPEZ O.P., FÉRIS L.A. Removal of reactive red 120 in aqueous solution using Mg-hydrotalcites as adsorbents solids: Kinetics and isotherms. Revista Internacional de Contaminación Ambiental. **36** (2), 443, **2020**.
35. AFMATAJ D., KORDERA O., MARAGKAKI A., TZANAKAKIS V.A., PASHALIDIS I., KALDERIS D., ANASTOPOULOS I. Adsorption of Reactive Red 120 Dye by Polyamide Nylon 6 Microplastics: Isotherm, Kinetic, and Thermodynamic Analysis. Water. **15** (6), 1137, **2023**.